Impact of Inherited Geometries on Syn-orogenic Foreland Basin Architecture

Benjamin Gérard, Delphine Rouby, Ritske Huismans, Cécile Robin, Charlotte Fillon, Jean Braun

Impact of Inherited Geometries on Syn-orogenic Foreland Basin Architecture

Benjamin Gérard[1], Delphine Rouby[1], Ritske Sipke Huismans[2], Cécile Robin[3], Charlotte Fillon[4] and Jean Braun[5,6]

[1]GET, Université de Toulouse, CNRS, IRD, UPS, Toulouse, France
[2]Department of Earth Sciences, Bergen University, Norway
[3]CNRS, Géosciences Rennes, UMR6118, University of Rennes, Rennes, 35042, France
[4]TotalEnergies, Centre Scientifique et Technique Jean Féger, Avenue Larribau, 64018 Pau Cédex, France
[5]Helmholtz Centre Potsdam, German Research Centre for Geosciences, Potsdam, Germany
[6]Institute of Geosciences, University of Potsdam, Potsdam, Germany

Corresponding author: Benjamin Gérard (benjamin.gerard.alpes@gmail.com)

Key Points:

- An initially elevated foreland domain produces a thinner flexural basin than a low-lying foreland domain as more sediments are exported.
- An initially deep foreland produces a thicker basin than a flat-lying foreland domain because of the extra load of the initial space infill.
- An initially deep foreland domain is required to preserve a significant proportion deep marine deposits in the foreland basin.

Abstract

We use a Landscape Evolution Model (FastScape S2S) to explore the impact of inherited topography in the foreland domain of a rising mountain range on its stratigraphic architecture and sediment accumulation history, inspired by the northern Pyrenean foreland. We simulate an uplifting half mountain range, its foreland basin and forebulge, and beyond, an open marine domain. We ran models with 4 different initial reliefs in the foreland domain: an initially flat foreland domain at sea-level, an elevated flat continental foreland (+300 m), a pre-existing 1 km-deep and 100 km-wide bathymetry at the location of the future foreland basin associated with a forebulge domain either at sea-level or elevated at +300m.

All models show a prograding mega-sequence associated with building of mountain topography and development of the flexural foreland basin and forebulge, coalescence of alluvial fans at the foot of the range, progressive continentalization of the foreland domain, and burial of the forebulge. An initially elevated foreland domain ultimately produces a thinner foreland basin while an initially deep foreland basin produces a thicker one.

After 10-13 Myr, the initial relief of foreland domain is smoothed out and the landscape does not exhibit a record of pre-existing relief. In contrast, the stratigraphic architecture of the foreland basin allows to trace inherited relief with deep marine sediments in the initially deep foreland basin, marine sediments onlapping and then burying the forebulge initially at sea-level, and continental sediments onlapping and burying the initially elevated foreland domain. We compare these interpretations to the Pyrenean retro-foreland.

Plain Language Summary

Rising mountain ranges thicken earth crust and, the extra load generates lateral depressions where sediments eroded in the mountain range are stored. This forms foreland sedimentary basins that record the growth of the mountain range. We simulated the landscape of a mountain range to test the impact of different initial relief of its foreland domain, before the mountain range build-up: initially low lying (0m), elevated (+300 m) or deep (-1000m) at the foot of the mountain range. We show that an initially elevated foreland will preserve less sediments and produce a thinner sedimentary basin than a low lying or deep forelands. The landscape smooth out inherited relief after ~10-13 Myr and cannot be used to infer it afterwards. As a difference, the geometry of the sediment strata in the basin are discriminant: with marine sediments covering the initially low lying and deep foreland and only continental sediments covering the initially elevated foreland.

1 Introduction

Foreland basins are unique archives of the evolution of orogenic mountain ranges as they preserve and recycle the products of their erosion. They often develop in previously rifted domain (Erdos et al., 2014) and while the impact of rifting on the deformation sequence has been widely studied (e.g. Molnar & Buiter, 2022; Wolf et al., 2021), its direct influence on the evolution of foreland basins in terms of sedimentary architecture remains poorly documented. The first-order stratigraphic architecture of foreland basins consists in most cases in a prograding and coarsening-up mega-sequence initiating with deep to shallow marine conditions, followed by continental fluvial plain and eventually alluvial fan deposits (DeCelles & Giles, 1996; Heller et al., 1988). This mega-sequence is controlled by the variation of the ratio of accommodation

space creation (A) and sediment supply (S) (Allen & Allen, 2005; Beaumont, 1981; Clevis et al., 2004; Dickinson, 1974), which are driven by tectonic growth of the mountain range, climatic variability and eustasy. The sedimentary mega-sequence in foreland basins exhibits three characteristic phases (Catuneanu, 2004; DeCelles, 2012). The "underfilled phase 1" is associated with deep marine depositional environments and an [A/S] ratio larger than 1. The filled phase 2 is associated with shallow marine and coastal fluvial plain depositional environments and an [A/S] ratio close or equal to 1. The overfilled phase 3 is associated with fluvial plain and alluvial fan depositional environments during which the [A/S] ratio is lower than 1.

Uplift and subsidence in foreland domains mainly result from the flexural isostasy response to the load of the topography of the growing mountain range forming a foreland basin at its foot and a distal forebulge. Sediment accumulation in the foreland basin further amplifies the flexural isostatic response, creating additional accommodation space in the foreland basin and uplift of the forebulge (Beaumont, 1981; DeCelles & Giles, 1996; Garcia-Castellanos & Cloetingh, 2012; Figure 1). Surface processes, as part of the sediment routing systems, constantly alter the topographic and sediment loads by producing sediments by erosion of the mountain range that are deposited in the foreland basins (Simpson, 2006). These mountain range-foreland basins systems are therefore complex source-to-sink systems controlled not only by mountain range tectonic uplift and foreland flexural subsidence but also by changes in climate, base-level and eustasy impacting erosion, sediment transport and deposition (Flemings & Jordan, 1989; Jordan & Flemings, 1991). Because these controlling factors are coupled, flexural isostatic numerical modelling including mass conserving diffusion-based erosion, sediment transport and deposition, has been commonly used to unravel their respective contributions on the stratigraphic evolution in foreland basins (see Paola, 2000 and Garcia-Castellanos & Cloetingh, 2012 for review). These studies have thoroughly analyzed, among others, the impact of erosional and depositional transport coefficients, effective elastic thickness, rate of thrust advance or sediment supply cycles on the development of the either long-term or short-term sequences and unconformities. For example, Flemings & Jordan (1989) showed that the transition from the underfilled to overfilled phases can be solely driven by surface processes (*i.e.* erosion, sediment transport and deposition efficiency) without other lithospheric processes in addition to the flexural isostasy. Sinclair et al (1991) showed that unconformities can develop in response to changes in thrusting and associated loading, the sediment transport coefficient, or the surface slope of the orogenic wedge without eustasy or complex viscoelastic lithosphere rheology. Flemings & Jordan (1990) demonstrated that thrusting events are recorded by transient retrogradations associated with deepening initiated at the onset of a thrust cycle within an overall progradation sequence. In addition to orogenic crustal thickening and sediment loading, an increase in displacement of the orogenic frontal fault combined with efficient erosion can produce a deeper foreland basin (Simpson, 2014). Finally, Naylor & Sinclair (2008) show that retro-foreland basins are stratigraphically more stable than pro-foreland basins as they exhibit a steady tectonic subsidence that allows recording the entire growth of the mountain range. Self-consistent thermo-mechanical models of mountain belt formation show similarly that shortening and outward growth predominantly occur in the pro-wedge, whereas the retro-wedge is largely stable (Erdos et al., 2014; Grool et al., 2019; Willett et al., 1993; Wolf et al., 2021).

Despite these numerous studies, the effect of inherited topography or bathymetry in the foreland domain on stratigraphic architecture has not yet been addressed. Mountain ranges often

115 develop in previously rifted domains, as for instance in Tethyan orogenic systems such as the
116 Pyrenees and the Alps (Desegaulx et al., 1991; Erdos et al., 2014; Schlunegger et al., 1997;
117 Vacherat et al., 2017). This suggests that these foreland domains may not correspond to flat
118 continental surfaces and exhibit pre-orogenic relief corresponding to remnants of the previous
119 extensional phase. In this work, we explore the effect of varying foreland paleo-topography and
120 paleo-bathymetry on foreland basin syn-orogenic stratigraphic architecture. To do this, we use a
121 Landscape Evolution Model taking into account both marine and continental sedimentary
122 processes and allowing to assess the relationships between stratigraphic architecture, flexural
123 isostasy, and landscape evolution in 3D (FastScape S2S; Yuan et al., 2019a; Yuan et al., 2019b).
124 We focus on the stratigraphic architecture of the retro-wedge foredeep, between the frontal tip of
125 the orogenic wedge and the forebulge (DeCelles & Giles, 1996). This allows us to simulate the
126 syn-orogenic landscape and foreland basin evolution with only vertical motion (uplift and
127 flexural isostasy) as retro-wedge systems of small to intermediate size orogens are relatively
128 stable and less affected by horizontal advection related to thrusting (Grool et al., 2018; Naylor &
129 Sinclair, 2008; Wolf et al., 2021). This generic approach, is inspired and compared to the
130 Pyrenean retro-foreland system in order to understand the potential effect of inherited
131 topography and/or bathymetry on the northern Pyrenean evolution and the build-up of its retro-
132 foreland.
133
134

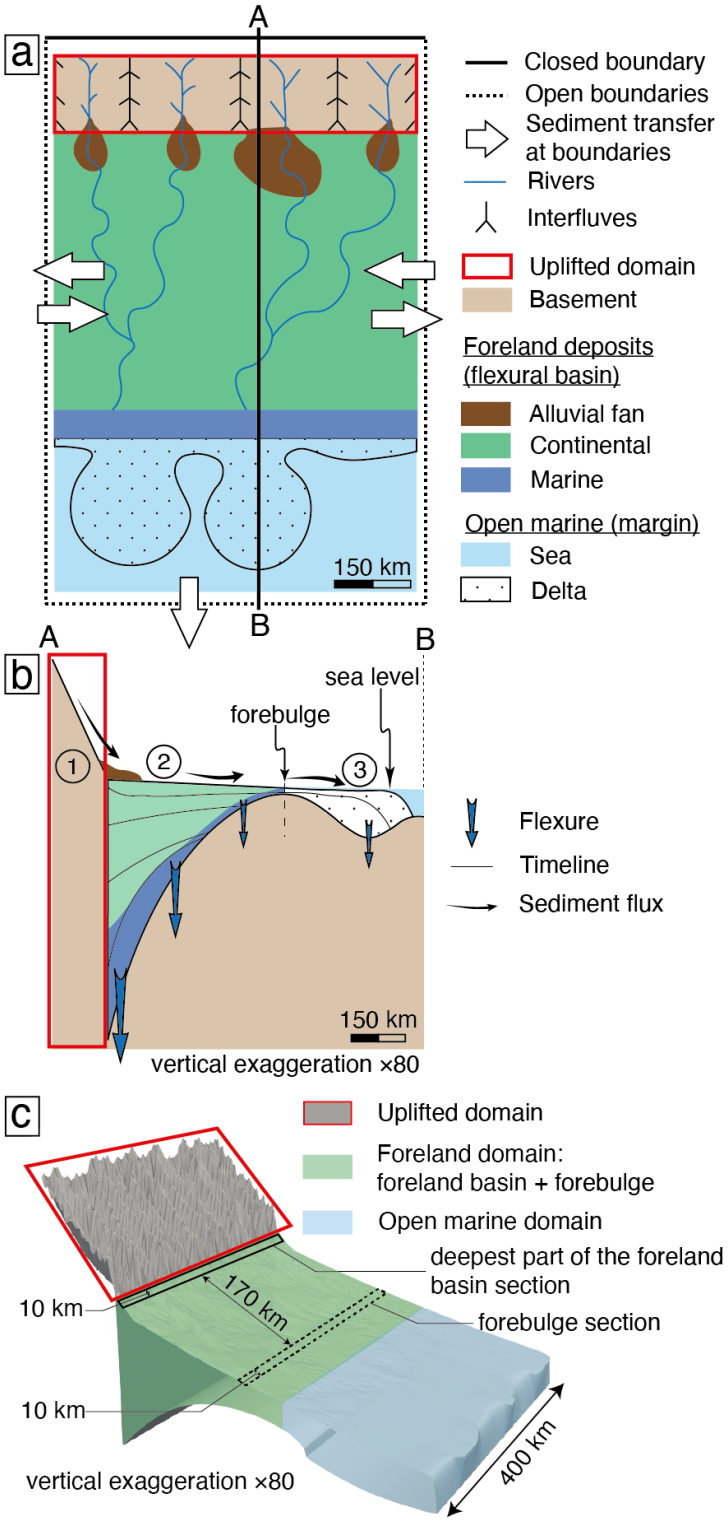

Figure 1. a) Top view of the model setup and associated landscape domains. Lateral open boundaries imply that sediments exiting the model on one side enter it back on the opposite side. b) Cross section (location in a) with (1) the uplifted domain, (2) the foreland domain (foreland basin and forebulge) and (3) the open marine domain. c) Perspective view of the model showing the location of the foredeep and forebulge sections.

2 Materials and Methods

We use the numerical Landscape Evolution Model FastScape (Bovy, 2021; Braun & Willett, 2013; Guerit et al., 2019; Yuan et al., 2019a; Yuan et al., 2019b). The model simulates the evolution of a fluvial landscape including sediment production, transport, continental and marine deposition, as well as the flexural isostatic response of the lithosphere to associated loading and unloading (Braun & Willett, 2013; Guerit et al., 2019; Yuan et al., 2019a; Yuan et al., 2019b; see details in Text S1).

Our model setup consists of a half mountain range (150×400 km) uplifting at a constant rate (0.5 mm/yr; Figure 1; Table 1) for 25 Myr. Eroded material produced in the uplifted area is transported to a foreland domain (350×400 km) and, beyond, to a distal open marine domain (200×400 km; Figure 1; Table 1). The foreland domain includes the foreland basin and the forebulge formed by flexural isostasy (Figure 1). The dimensions of the models are consistent with small-orogen retro wedge systems.

We present four models with varying initial topography and bathymetry in the foreland (Figure 2): Reference model M1 with a foreland domain initially at sea-level (Figure 2a); Model M2 with a foreland domain elevated at +300 m (Figure 2b); Model M3 with a 100 km-wide and 1000 m-deep water filled foreland basin and a 250 km-wide forebulge area at sea-level (Figure 2c); Model M4 with a 100 km-wide and 1000-m deep water filled foreland basin and an elevated foreland area 300 m above sea level (Figure 2d). Model M1 is a reference model to allow comparisons. Initial bathymetries in models M3 and M4 are comparable to rift remnants as often encountered in natural orogenic systems such as the Pyrenees (e.g., Desegaulx et al., 1991). The initially elevated foreland domain in models M2 and M4 represents stable Phanerozoic continents that have an average elevation of ~400 m +/- 400 m (e.g., Theunissen et al., in review). The initial bathymetry in models M3 and M4 represents pre-existing rift related topography. To initiate river grading toward the foreland domain, we impose a small initial tilt of the uplifted domain ($\alpha = 0.076°$; Figure 2).

In the four models, we use parameter values generally admitted in the literature (Table 1). A constant and homogenous precipitation rate P = 0.5 m/yr, an effective elastic thickness, EET = 15 km, fluvial erodibility $K_f = 2.5\times10^{-5}$ $m^{0.2}$/yr (Whipple & Tucker, 1999), hillslope diffusion $K_h = 1.0\times10^{-2}$ m^2/yr (Armitage et al., 2013; Densmore et al., 2007), continental deposition coefficient G = 0.4 (Davy & Lague, 2009; Guerit et al., 2019), and a marine diffusion coefficient $K_d = 2.0\times10^{2}$ m^2/yr (Jordan & Flemings, 1991; Rouby et al., 2013; Yuan et al., 2019b; Table 1). For marine diffusion, we use value representative for a silty grain-size (Rouby et al., 2013; Simon et al., in review). Sediment compaction is not included.

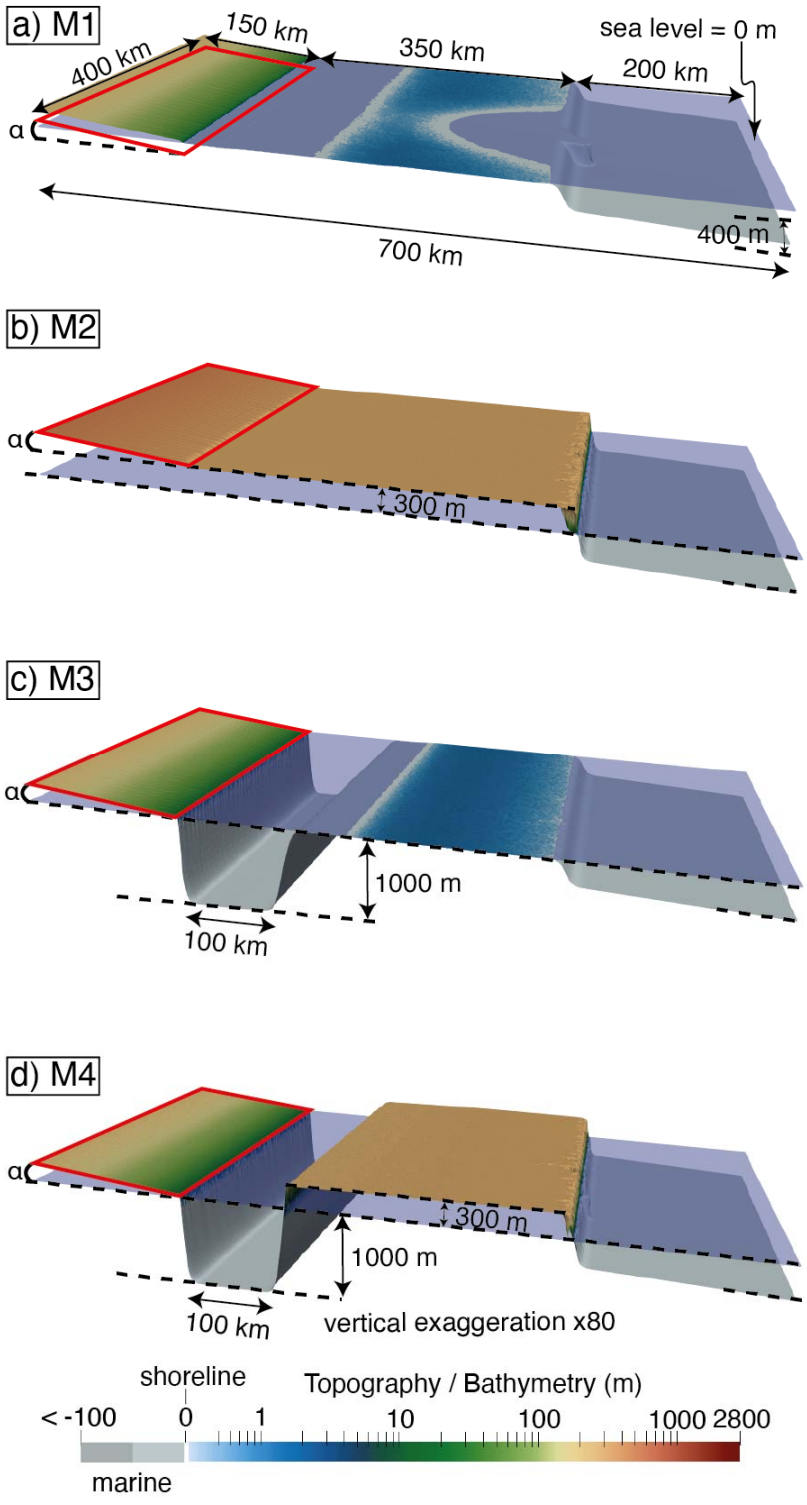

Figure 2. Setup for models M1-M4. a) M1, foreland domain at sea-level. b) M2, elevated foreland domain (+ 300 m). c) M3, the foreland domain is composed of a water filled foreland basin (100 km wide; 1000 m deep) and forebulge at sea-level (250 km wide). d) M4, the foreland domain is composed of a water filled foreland basin (100 km wide; 1000 m deep) and an elevated forebulge at sea-level (250 km wide; + 300 m). Initial slopes of the uplifted domains (red box) are identical ($\alpha = 0.076°$).

186 **Table 1**. *Common Parameters for the Different Models*

Parameter	Value	Unit
Size of the model domain	400×700	km
Size of the cell (d_x, d_y)	1000	m
Time step (d_t)	1000	yr
Total duration	25×10^6	yr
Uplift rate (U)	0.5	mm/yr
Precipitation rate (P) - homogeneous and constant	0.5	m/yr
Effective Elastic thickness (EET)	15[a]	km
Erodibility (K_f)	2.5×10^{-5} [b]	$m^{0.2}$/yr
Hillslope diffusion coefficient (K_h)	1.0×10^{-2} [c;d]	m^2/yr
Deposition coefficient (G)	0.4[e;f]	-
Erosion law coefficients (m, n)	0.4[g], 1[h]	-
Sea-level elevation	0	m
Marine diffusion coefficient (K_d)	2.0×10^2 [i;j;k;l]	m^2/yr
Porosity (∅) - proxy for compaction	0	%

187 *Note.* The erodibility value (K_f) was chosen to reach a mean mountain range elevation of ~1.7
188 km after 25 Myr. Parameters from [a]Garcia-Castellanos & Cloetingh (2012); [b]Whipple & Tucker
189 (1999); [c]Densmore et al. (2007); [d]Armitage et al. (2013); [e]Davy & Lague (2009) ; [f]Guerit et al.
190 (2019) ; [g]Stock & Montgomery (1999); [h]Braun & Willett (2013); [i]Jordan & Flemings (1991);
191 [j]Rouby et al. (2013); [k]Yuan et al. (2019b); [l]Simon et al. (in review).
192
193 **3 Results**
194 **3.1 Reference model M1**
195 During the first 1 Myr of the reference model M1, initial mountain belt grows to an
196 average topography of 1.7 km elevation at 25 Myr (Figures 3a and 4a). The basement of the
197 flexural foreland basin subsides progressively under the load of the mountain range topography
198 and of the deposited sediments. The depositional environments are largely shallow marine and
199 the forebulge is partly submerged (Figures 3b and 4a). Part of the sediments produced by erosion
200 of the mountain belt fills the flexural foreland basin while the remainder is exported to the
201 marine domain ([A/S] ratio less than, but nearly equal to, 1; Figures 3a and 4a). Initially isolated
202 and progressively coalescing alluvial fans (sediment deposited at a slope > 0.4°; Bull, 1964;
203 Milana & Ruzycki, 1999) form at the foot of the mountain range (Figures 3b and 4a). At 6 Myr,
204 continental deposits migrate from the foot of the mountain range to the forebulge as the foreland
205 basin evolves toward an overfilled stage ([A/S]<1; Figures 3b and 4a). At 15 Myr, continental
206 deposits reach the forebulge (Figures 3c and 4a). At 25 Myr, the foreland domain is completely
207 continentalized and the forebulge area is emerged (Figures 3d and 4a).
208

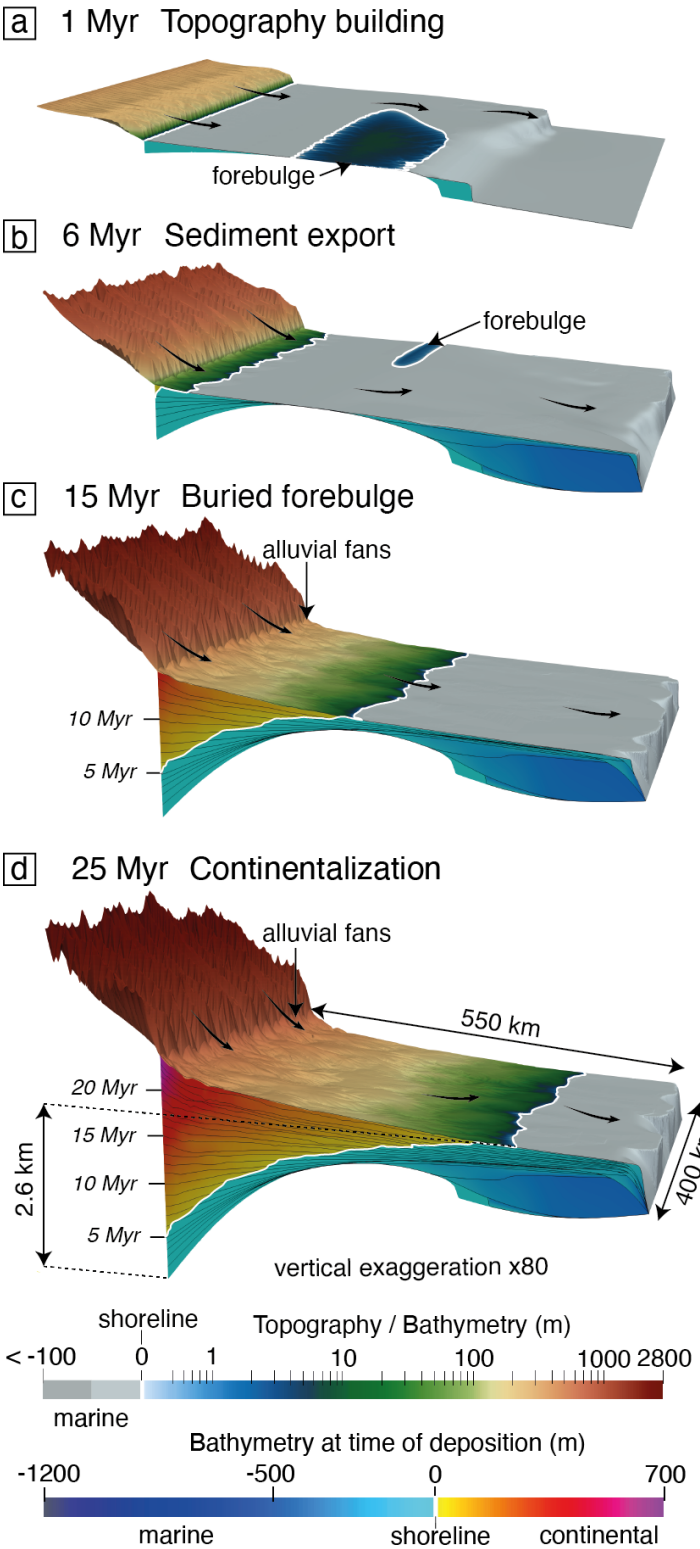

Figure 3. Evolution of model M1 at (a) 1 Myr; (b) 6 Myr, (c) 15 Myr and (d) 25 Myr. The surface of the model is coloured according to the topography and bathymetry. The section of the model is coloured according to the depositional bathymetry. Black arrows represent sediment transport directions.

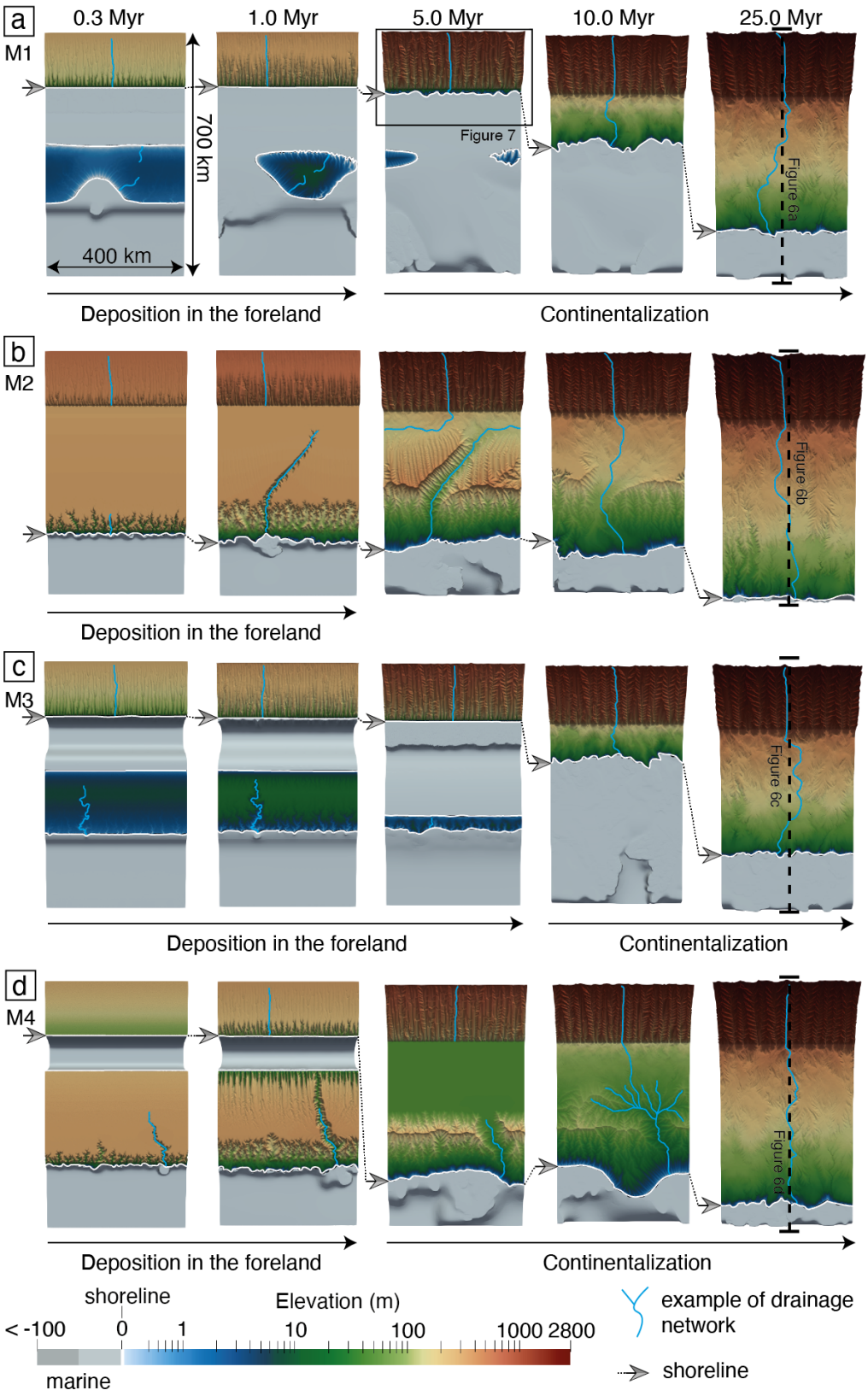

Figure 4. Top view of the topography of models (a) M1, (b) M2, (c) M3 and (d) M4 at 0.3, 1, 5, 10 and 25 Myr. Topography below sea-level is shown in grey.

3.2 Models M2 to M4 with inherited topography/bathymetry in the foreland domain

Models with inherited topography and/or bathymetry in the foreland domain follow a general first order evolution similar to the reference model: initial building of mountain range topography, development of the flexural foreland basin, formation of alluvial fans at the foot of the mountain range, and the progressive continentalization of the foreland domain (Figures 4, S1, S2 and S3). Inherited topography and/or bathymetry in the foreland domain does nevertheless have a significant impact on the surface evolution of the models (Figures 4, S1, S2 and S3).

Model M2, that has a continental foreland domain initially elevated at 300 m (Figure 2b), develops a drainage network that incises the foreland domain and connects the mountain range to the open marine domain within the first 5 Myr (Figures 4b and S1). Throughout the model evolution, the subsiding foreland basin preserves part of the sediments deposited in a continental environment, while the remaining sediments are exported to the open marine domain. In contrast with the reference model M1, the initially open marine domain is entirely continentalized after 25 Myr (Figures 4b and S1).

Model M3 includes an initial water filled foreland basin (1000 m deep) at the foot of the uplifting mountain range (Figure 2c). During the first 5 Myr, sediments produced in the mountain range are fully stored in the initial deep basin under marine depositional conditions (Figures 4c and S2). At this stage the foreland basin is underfilled ([A/S]>1). The export of sediments toward the open marine domain and the transition to an overfilled stage ([A/S]<1) are delayed compared to the reference model M1 (Figures 4a, 4c and S2).

Model M4 combines an initial water filled foreland basin at the foot of the uplifting mountain range with a continental forebulge initially elevated at 300 m (Figure 2d). During the first 5 Myr, sediments are fully stored in the initial deep basin, under marine depositional environments, similarly to model M3 (underfilled stage; [A/S]>1). Additional sediments are, however, produced by erosion of the elevated forebulge area and deposited in the foreland and in the marine domain (Figures 4d and S3). Similarly, to M3, sediment export toward the open marine domain is delayed compared to the reference model M1 (Figures 4a, 4d and S3). The foreland basin reaches the overfilled stage with continental depositional environments by 5 Myr, earlier than in the reference model M1 (Figures 4a, 4d and S3). After 10 Myr, erosion affects the continental foreland domain, remobilizing and exporting previously deposited sediments towards the open marine domain. The entire foreland domain is continentalized at 25 Myr (Figure 4d).

3.3 General characteristics of mountain range and foreland basin evolution

We next evaluate the evolution of mean elevation, mean erosion rate, foreland basin depth, and sediment volume in the models (Figure 5). The evolution of the mean elevation of the uplifted domain is very similar in the four models and shows a progressive build-up to ~1.7 km after 25 Myr, without reaching steady state (Figure 5a). Associated mean erosion rates in the mountain range follow a similar build-up to 3.5 - 4.0×10^{-4} m/yr at 25 Myr (Figure 5b). During this build up however, all models undergo drops in mean erosion rates (ca. two-fold decrease; Figure 5b). The timing of the drops in erosion rate varies from one model to the other (5.2, 4.9 and 3 Myr in Models 1, 2 and 3 respectively). Model M4 shows a more complex behavior with a first drop at 4.6 Myr and a second one at 11.9 Myr associated with a few oscillations. After the drops, all models return to a trend of increasing mean erosion rates over time (Figure 5b). This

particular behavior is further discussed below. Supplementary Figure S4 provides a top view of the erosion and deposition rates above sea-level through time.

The maximum basement depths of the foreland basins of M1 to M4 exhibit similar deepening trends but reach different final depths at 25 Myr (e.g., 2.7 km for M1, 2.3 km for M2, 3.6 km and 3.4 km for M4; Figure 5c). The total volume of sediments produced in the mountain range is similar in the four models (4 to 4.5×10^{14} m^3). However, the volume of sediment accumulated in the foreland is quite different between the models (1.30×10^{14}, 0.95×10^{14}, 2.20×10^{14} and 1.80×10^{14} m^3 for M1, M2, M3 and M4 respectively; Figure 5d). This is mirrored by different proportions of sediments exported to the open marine domain.

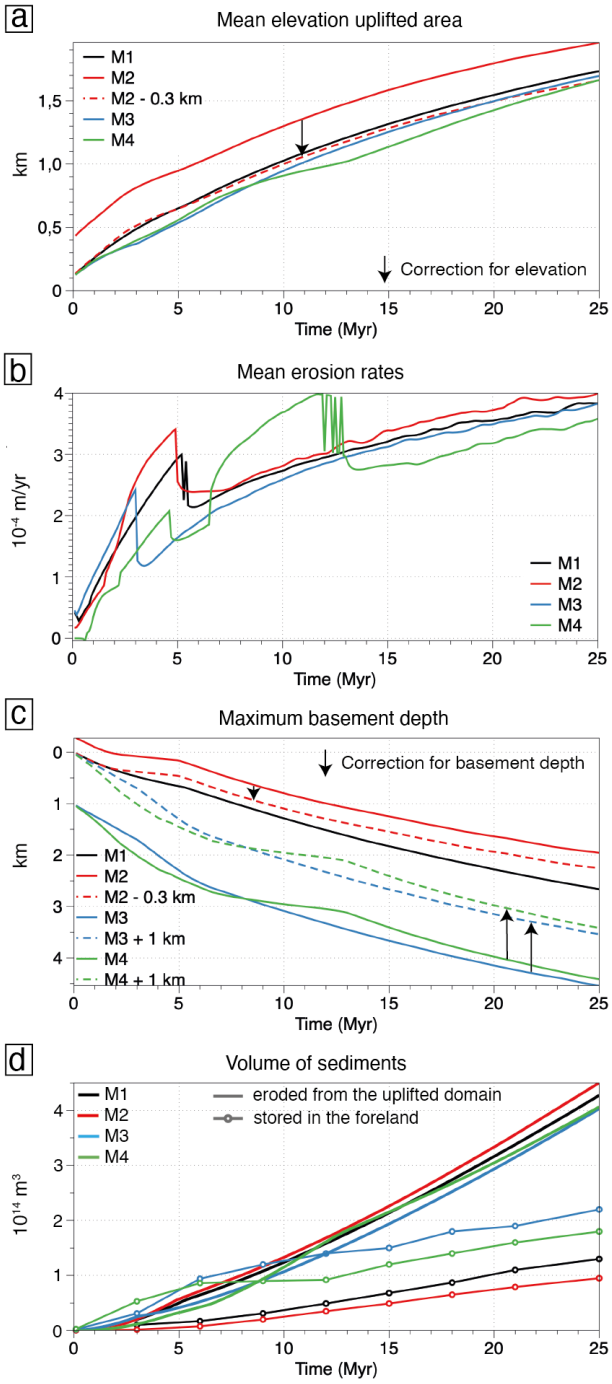

Figure 5. a) Mean elevation of the uplifted domain of the four models through time. Dashed line for M2 is the elevation normalized to the other models, i.e., corrected for additional topography (-300 m). b) Mean erosion rates of the uplifted areas of the four models. c) Maximum basement depth in the foreland of models (foredeep section, see location in Figure 1c). Dashed lines for M2, M3 and M4 are the basement depths normalized to the other models, i.e., corrected for topography (-300 m) or additional bathymetry (+1000 m). d) Cumulative volumes of sediments produced in the mountain range (solid lines) and stored in the foreland basins (dotted lines). For models M3 and M4, volumes stored in the foreland basin are corrected from the volume of the initial bathymetry (40 000 km^3).

3.4 Foreland basin stratigraphic architecture

For each model, we show the stratigraphic architecture of the foreland basin along a longitudinal cross-section as well as the corresponding Wheeler diagram of the depositional bathymetry/elevation through time (Figures 6a-h; Sections location in figure 4). We highlight the transition from alluvial fan to fluvial plain deposits for sediments with a depositional slope > 0.4° (Figures 6 and S5; Bull, 1964; Milana & Ruzycki, 1999).

In reference model M1, the foreland basin has a maximum thickness of 2.6 km at the mountain front (Figure 6a). It shows continuous accumulation, first in a shallow marine depositional environment with a water depth <100 m and an [A/S] ratio >1, evolving to continental conditions with a [A/S] ratio <1 (Figures 6a and 6e). Marine foreland basin deposits first onlap the forebulge before burying it by 12 Myr (Figures 6a and 6e). Continental deposits emplaced at the foot of the mountain range from 5-7 Myr and then progressively propagate through the foreland domain to reach the open marine domain by 25 Myr. Alluvial fans propagate up to 40 km within the foreland basin (Figures 6a and 6e).

In model M2, sediments in the foreland basin are significantly thinner than in reference model M1, reaching a maximum thickness of 2.0 km of only continental deposits (Figure 6b and 6f). Significant regressive erosion affects the elevated foreland until 10 Myr (Figure 4b and 6f). Continental sediments bury the forebulge by 11 Myr (Figures 6b and 6f). The foreland shows several local incisions, especially after 16 Myr (Figure 6f). The erosion patterns of fluvial incision (channels of a few kilometers) or larger eroding areas (~80 km) develop particularly above the buried forebulge, remobilizing previously deposited sediments (Figure 6f). Alluvial fans propagate up to ~100 km within the foreland basin (Figures 6b and 6f).

In model M3, the foreland basin reaches a maximum thickness of 4.5 km (Figure 6c). Sediments produced in the mountain range are initially fully deposited in the deep foreland basin under marine environments with water depths >300 m and an [A/S] ratio >1 (Figure 6c). The marine sediments progressively onlap the forebulge before burying it by 10 Myr (Figure 6c and 6g). Subsequently, the shoreline propagates across the foreland domain similarly to model M1 (Figure 6g). Alluvial fans then propagate up to ~80 km within the foreland basin (Figures 6c and 6g).

In model M4, the maximum thickness of the foreland basin is 4.4 km, similar to model M3 (Figure 6d). The initial deep foreland basin is under marine depositional environments until 5 Myr, with deposition depth >300 m (Figure 6d). The transition to overfilled conditions ([A/S] ratio <1) occurs earlier than in reference model M1. At 13 Myr the forebulge is buried by continental deposits (Figure 6h). Similar to Model M2, the elevated forebulge undergoes significant regressive erosion until 10 Myr (Figures 4d and 6h), and shows more local incisions afterwards, at 12 and 22-23 Myr (Figure 6h). Subsequently, alluvial fans propagate for more than 100 km in the foreland basin (Figures 6d and 6h).

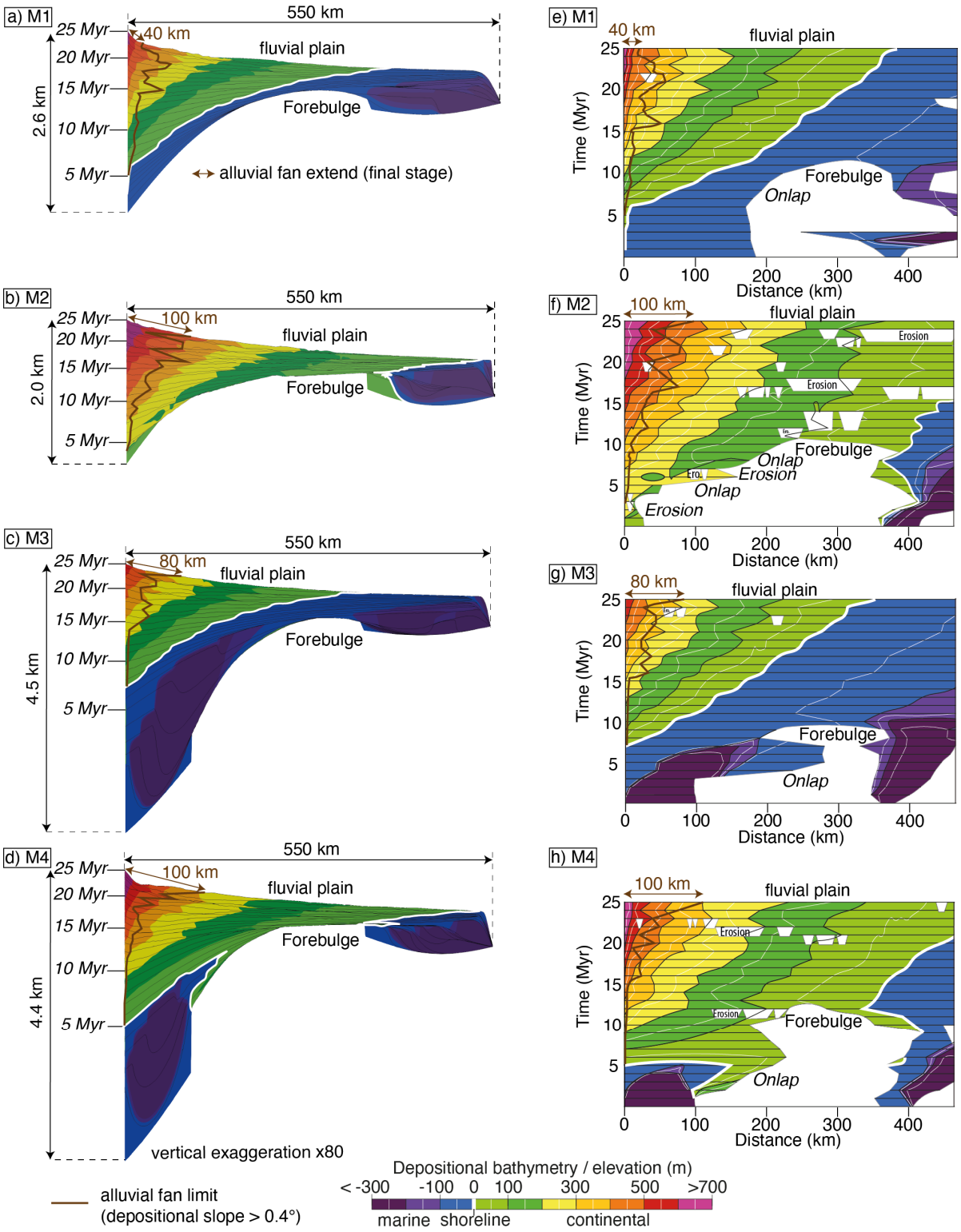

Figure 6. Stratigraphic architecture of the foreland basins of (a) M1, (b) M2, (c) M3 and (d) M4 models along the sections located in Figure 4. Sediments are coloured according to their depositional bathymetry or elevation. Associates Wheeler diagrams of (e) M1, (f) M2, (g) M3 and (h) M4 models. The limit between fluvial plains and alluvial fans is extracted for portions, longer than 10 km, associated to depositional slopes >0.4° (Figure S5).

3.5 Erosion and accumulation dynamics

Our models show peculiar erosion and accumulation features. In reference model M1, erosion rates in the mountain range reduce sharply at 5.2 Myr. Subsequently the rate of erosion increases again steadily with time (Figures 5b and 7). The reduction in erosion rate is coeval with the coalescence of alluvial fans at the foot of the mountain range (Figure 7b). Models M2-M4 exhibit similar behavior with one or more short time scale reductions of erosion rate that are also correlated to changes in continentalization or alluvial fan dynamics (Figure 5b, S6, S7 and S8).

Figure 8 shows the co-evolution of depositional environments and bathymetry/elevation at the foot of the mountain range. In models M1, M3 and M4, transition from marine to continental depositional environments occurs between 3.0 and 4.6 Myr. In model M1, M2 and M3, alluvial fan build-up occurs between 4.9 and 6.0 Myr. Model M4 presents specific features in comparison to other models. Transition from marine to continental depositional environments corresponds to a first alluvial fan build-up (*i.e.*, without preceding fluvial plain deposits) and a second phase of alluvial fan build-up occurs at 11.9 Myr (Figure 8d). The shoreline migration rates across the foreland are 23 and 17 km/Myr for M1 and M3, respectively (Figures 8a and 8c). For all models, the maximum elevation of the alluvial fan varies from 600 to 800 m at 25 Myr (Figures 8).

Interestingly, reductions in erosion rates in the mountain range are coeval with the transition from the underfilled to the overfilled phase, that is with the transition from marine to continental depositional environments and/or with alluvial fan coalescence in the foreland basin (Figures 5b, 7, 8, S6, S7 and S8).

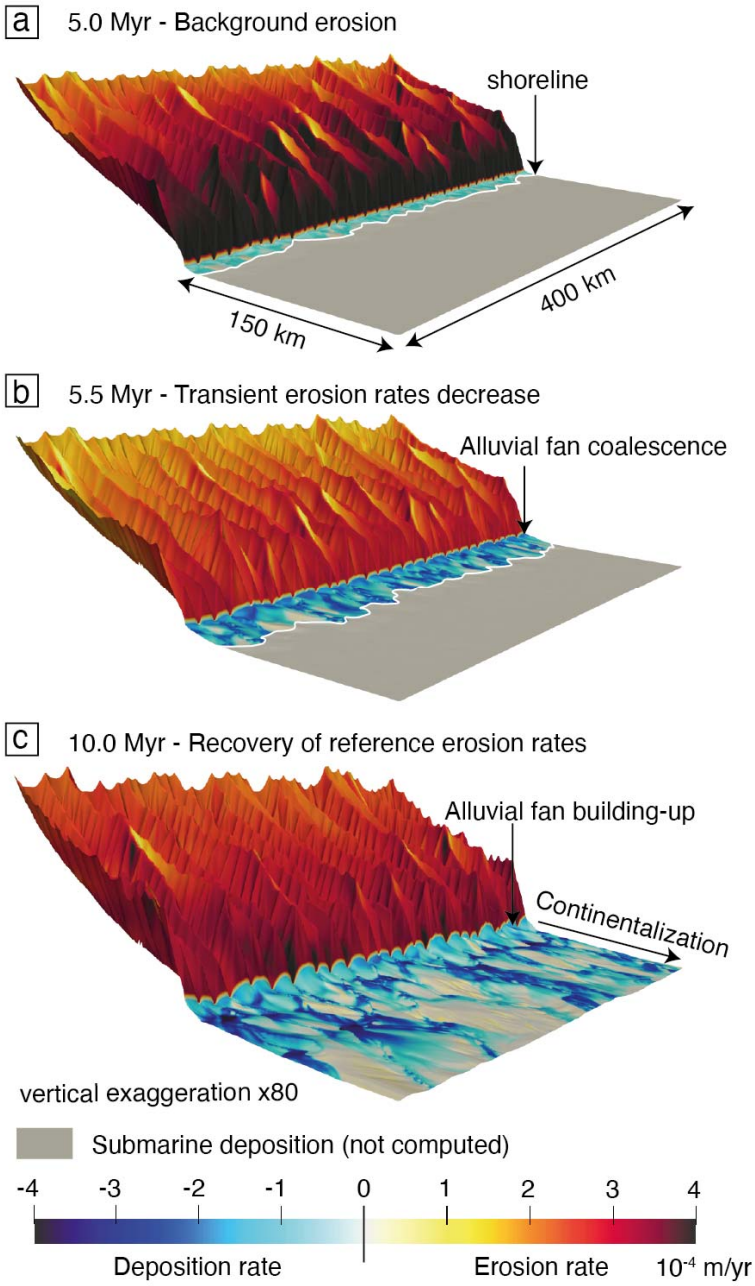

Figure 7. Zoom of the erosion and deposition rates of model M1 in the uplifted mountain range and proximal foreland domain at a) 5 Myr (alluvial fan build-up initiation), (b) 5.5 Myr (alluvial fan coalescence), and c) 10 Myr (after alluvial fan coalescence). Note the decrease in erosion rates in the uplifted area around 5.5 Myr. See location of the zoom area in Figure 4a.

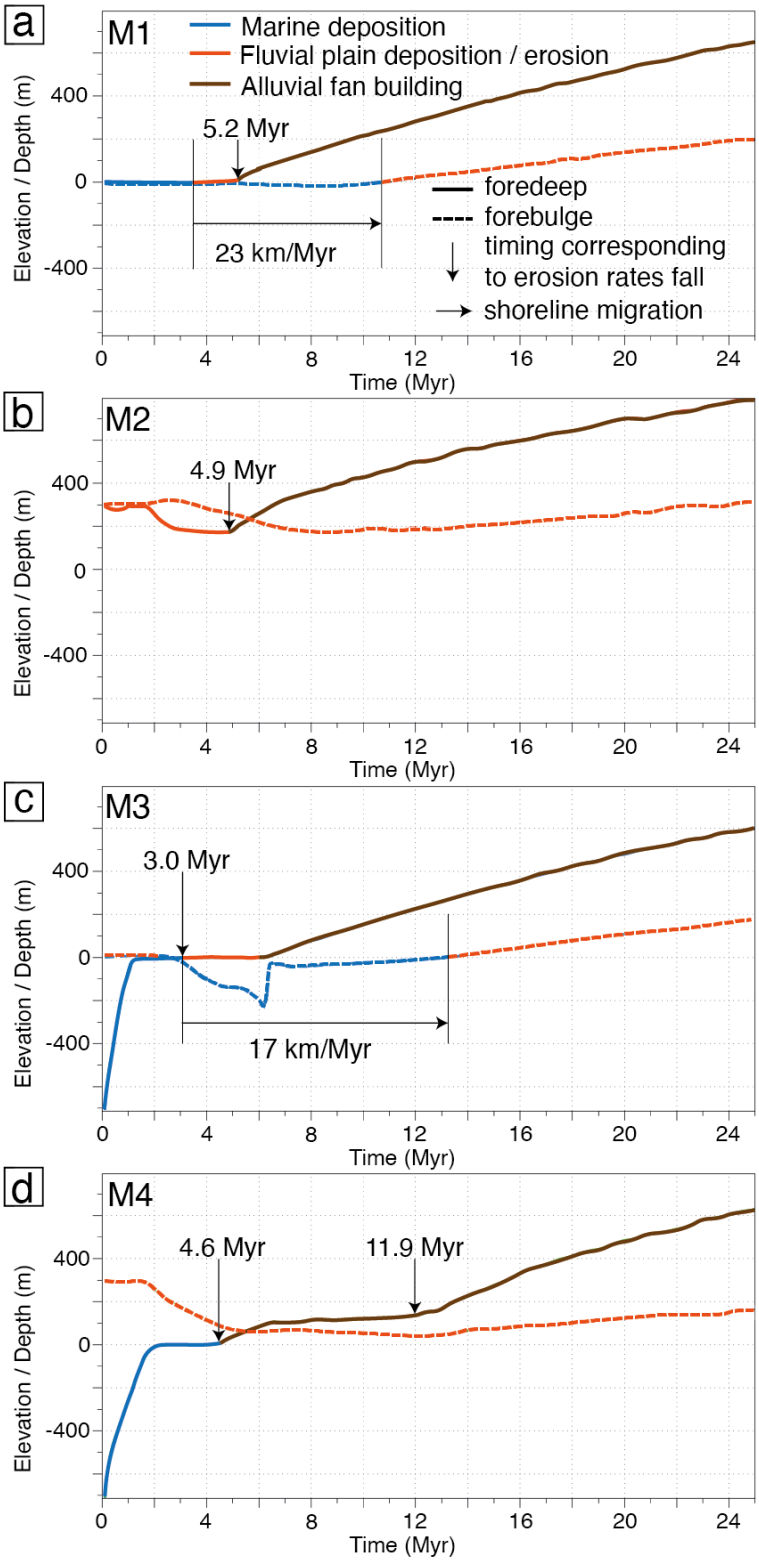

Figure 8. Evolution of depositional bathymetry / elevation of sediments at time of deposition along the foreland section (solid line) and forebulge section (dashed line; see location of sections in Figure 1c) for models M1 to M4 (Figure 2). These curves represent the mean elevation values integrated along the sections (Figure 1c).

4 Discussion

4.1 Stratigraphic evolution trends of reference model M1

Model M1 produces a long-term prograding mega-sequence that is characteristic of foreland basin stratigraphic architecture (Figure 9a; DeCelles & Giles, 1996). During the first stage, the topographic load of the rising mountain range creates accommodation in the foreland basin by flexural isostasy allowing storage of sediments at the foot of the mountain range (Figures 5a, 5b, 3 and 6a). The load of these sediments amplifies the flexural subsidence of the foreland basin. At the same time, sediments in excess of accommodation space available in the foreland basin are exported across the forebulge to the open marine domain (Figure 3a). The foreland basin at the foot of the mountain range is characterized by marine depositional environments between 0-3.6 Myr corresponding to the underfilled phase ([A/S]>1; Figures 3a and 8). From 3.6 Myr onward, the foreland basin stores progressively less sediments showing that creation of accommodation space by flexure is lower than sediment production in the mountain range (Figure 5d). The progressive continentalization of the foreland domain initiated at 3.6 Myr marks the transition of the foreland basin from underfilled to filled-overfilled ([A/S]≤1; Figures 3 and 8a). This transition is slightly diachronous longitudinally, depending on the local relief of the mountain range, and migrates across the foreland basin at a mean rate of 23 km/Myr (Figures 3, 6a, 6e and 8a). Models M2 to M4 display this long-term trend as well, although the timing of continentalization and sediments export to the marine domain are different (Figures 6 and 9).

Along with the continentalization, alluvial fans form at the foot of the range and show alternating build-up and retreat away and toward the mountain range (Figures 6a and 6e; Catuneanu, 2019). These oscillations are driven by local lateral migration of alluvial fans (i.e., in and out of the cross-section). These lateral migrations are driven by the competition between local erosion and the space available for deposition, which is controlled by the deposition of the previous fans, local reliefs and individual drain dynamic (Movie S1). These short-term oscillations provide only minor perturbations within the general long-term prograding mega-sequence in which alluvial fans migrate from the mountain range towards the open marine domain (Figure 9).

All our models are based on identical mountain range uplift rate, erodibility, and effective elastic thickness. To test the robustness of the mega-sequence described above, we performed a sensitivity analysis of model M1 to varying uplift rate, erodibility, and effective elastic thickness. Varying these parameters modifies the timing of the characteristic stages of the mega-sequence (Table S1; Figures S9 to S11). Supplementary model SM1 shows that higher uplift rate results in higher mountain range topography and accordingly topographic load, which result in a larger flexural isostatic response of the foreland and ultimately in thicker foreland basin deposits (Figure S9). Supplementary model SM4 shows that higher erodibility reduces mountain range topography and the associated flexural controlled accommodation space creation in the foreland basin (Figure S10). Finally, supplementary model SM5 shows that higher effective elastic thickness results in higher amplitude and longer wavelength of foreland basin deepening, resulting in a thicker foreland basin (Figure S11). However, the long-term stratigraphic mega-sequence of the foreland basins described above is similar in all our models irrespective of the uplift rate, erodibility, and effective elastic thickness (Text S2; Table S1; Figures S9 to S11).

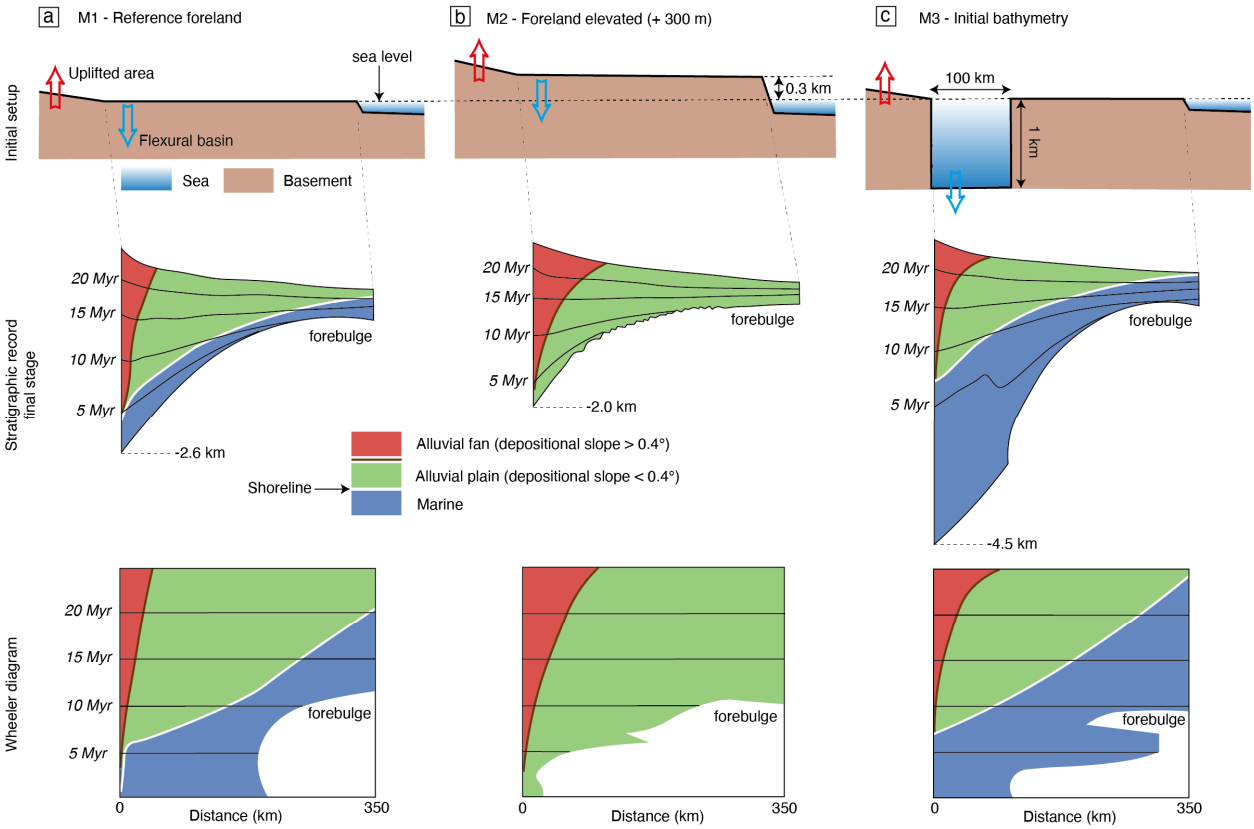

Figure 9. Schematic stratigraphic architecture for models (a) M1, (b) M2 and (c) M3. Upper panels show schematic cross-sections of the initial setups. Middle panels show schematic cross-sections of the depositional environments in the foreland basin. Bottom panels show associated schematic Wheeler diagrams.

4.2 Influence of inherited foreland domain topography and bathymetry

The landscape evolution of models M1 to M4 is significantly different within the first 10 Myr as a result of the inherited foreland domain bathymetry and topography (Figure 4). For instance, in cases with a pre-existing foredeep (e.g., M3 and M4), sediment export to the open marine domain is delayed with respect to reference model M1 because the initial deep basin first fills-up during the first 4 - 7 Myr (Figure 4 and 5d; Movies S3 and S4). In models with an elevated foreland (M2 and M4), regressive erosion remobilizes sediments previously deposited in the foreland domain (Figures 4b and 4d; Movies S2 and S4). The forebulge is buried by continental sediments in models with an elevated foreland while it is buried by marine sediments when the foreland domain is initially at sea-level (models M1 and M3; Figures 6 and 9; Movies S1 and S3). However, the influence of the initial relief largely disappears after ~10-13 Myr and all models show similar landscapes with a continentalized foreland domain developing longitudinal hydrographic networks (Figure 4). Nonetheless, at 25 Myr, the location of the shoreline in the various cases provides a memory of the initial foreland basin setting. An initial elevated foreland leads to further migration of the shoreline compared to the reference case. Thus, in our models, the landscape after 10-13 Myr contains only indirect clues regarding the initial foreland geometry (Figure 6).

Once the foreland basin is continentalized, the sedimentary load is more evenly distributed over the entire accumulation area (foreland basin, forebulge, and open marine domain). Its influence on the flexure and the differential subsidence/uplift in the foreland basin and forebulge decreases (Figure 5). On the other hand, the increasing topographic load of the mountain range continues to deepen the basement of the foreland basin. Over time the importance of local flexural isostatic subsidence decreases, especially when the forebulge is permanently buried by sediments (between 10 and 13 Myr in the models shown here; Figures 6 and 9). This stage corresponds to the period when the initial topography and bathymetry are no longer visible in the landscape.

The initial relief of the foreland does not significantly influence the topographic evolution of the mountain range and, accordingly, mean elevation histories are similar in the four models (Figure 5a). As the mean elevation of the uplifted domain and sediment production are similar between the models, the topographic load of the mountain range cannot explain the differences in the depth of the foreland basin basement in the four models (Figure 5c). The differences in foreland basin geometry are consequently directly linked to the load of the sediments stored in the foreland basin and to variations in accommodation space creation resulting from different initial topography and bathymetry of the foreland domain.

4.3 Influence of the initial elevation of the foreland domain on its stratigraphic evolution

The initial elevation of the foreland domain directly controls its storage capacity for sediments. In models with an initial foreland domain at sea-level (M1 and M3), the foreland basin basement is ultimately 600 m deeper and has a thicker infill with a large proportion of marine to continental sediments than in models that have a foreland domain that is initially elevated (M2 and M4; Figures 5c and 6). The initially elevated foreland domain (300 m above marine base-level) is rapidly incised by regressive erosion that connects the mountain range to the open marine domain (Figures 4b and 4d). These river networks, not only export sediments exiting the mountain range to the marine domain, but also remobilize sediments previously stored in the foreland basin (Figures 4b, 4d, 6 and 9).

The initial elevation of the foreland domain also influences the build-up of alluvial fans at the foot of the mountain range. Alluvial fans form at higher elevation and are more widely spread out at the foot of the mountain range in models with an initially elevated foreland domain (~100 km for M2 and M4) than in models with a foreland domain at sea level (< 80 km for M1 and M3; Figures 6, 8 and 9). We interpret this to result from reduced accommodation space available in the case of an initial elevated foreland domain that allows less material to be stored at the foot of the mountain range in comparison with cases with a foreland domain at sea level. The lower amount of sediment stored in the foreland basin for these cases results in less accommodation space creation by flexure. As a result, alluvial fans form at higher elevation in an initially elevated foreland and spread further out than in cases with a foreland domain that is initially at sea level.

4.4 Influence of an initially deep foreland basin on its stratigraphic evolution

In models M3 and M4 with an initially deep foreland basin (1000 m), the basement is twice deeper and sediments are twice thicker than in models with a foreland initially elevated or

at sea-level (M1 and M2; Figures 5c, 6 and 9). The initially deep foreland basin forms a large additional accommodation space. Sediments exiting the mountain range that are initially stored in the inherited deep foreland basin increase the load induced flexural response and the creation of accommodation space with respect to the models without a deep basin (M1 and M2; Figures 4, 5c and 6). Sediment export to the open marine domain is accordingly delayed and the foreland domain is less incised when it emerges (Figure 6). Accordingly, shoreline migration across the foreland domain and continentalization are slower for model M3 (17 km/Myr) than for reference model M1 (23 km/Myr; Figure 8). In addition, our models suggest that an initially deep foreland basin is required to preserve a significant proportion of marine deposits in foreland basins.

The initially deep foreland basin also leads the formation of alluvial fans at lower elevation than in other models (Figures 6 and 8). In the cases with an initial deep foreland basin, the additional load of sediments filling in the basin enhances the flexural response and the creation of accommodation space (Figures 5c, 6 and 9). As a result, the continentalization rate is slower and alluvial fans form at lower elevations than in the reference model.

As discussed by Simpson (2014), increased displacement of the mountain range-fault front leads to a deeper foreland basin. We show here that an inherited bathymetry, which can be considered as a rift remnant, provides an alternative mechanism to produce a deep foreland basin.

4.5 Accumulation feedback on erosion rates

We show above that the inherited foreland domain topography and bathymetry exert a control on the sediment accumulation history in foreland basins in a syn-orogeny context. However, the filling dynamics of the foreland basin also exerts a feedback on erosion of the mountain range. Indeed, abrupt drops in erosion rates in the uplifted domain (Figures 5b and 7) are synchronous with changes in the depositional systems at the foot of the mountain range in the foreland domain. These systematically correspond to a transition from marine to continental depositional environments or from fluvial to alluvial fan deposits (Figures 7, 8, S6, S7 and S8).

Continentalization of the foreland domain, as well as build-up and coalescence of alluvial fans, is associated with a raise of the base-level at the foot of the mountain range resulting in a decrease of the erosive potential of the mountain range (Babault et al., 2005; Carretier & Lucazeau, 2005). These events are responsible for the transient drops of erosion rates observed in the mountain range (Figures 5b and 7). Afterwards, the hydrographic network returns to its previous base level and erosion rates in the mountain range gradually return to similar but lower trends (Figure 5b). This autogenic feedback has previously been documented using both analogue (Babault et al., 2005) and numerical modelling studies (Carretier & Lucazeau, 2005). The high-frequency transient oscillations in erosion rates shown in models M1 and M4 correspond to short time scale coalescence and dispersal events of alluvial fans (< 500 kyr; e.g., Figure 5b). However, these short-term oscillations do not impact the long-term erosion dynamics of the mountain range.

4.6 Comparison with the Pyrenean retro-foreland system

We next consider the northern retro-foreland system of the Pyrenees (Figure 10). The northern Pyrenees and the Aquitaine basin – Bay of Biscay system is a classic example of retro-

wedge flexural foreland basin (Angrand et al., 2018; Bernard et al., 2019; Ortiz et al., 2020). The northern Pyrenean retro-foreland developed through inversion of an inherited rifted domain. Vacherat et al. (2017) and Desegaulx et al., (1991) show that inherited bathymetry in the Pyrenean proto-foreland significantly affects the record of vertical motion and the stratigraphy of the foreland. The Pyrenean retro-foreland basin exhibits a classical prograding coarsening upward megasequence (Ortiz et al., 2020). Several features of the Pyrenean system are, however, not included in our model setup such as: horizontal displacement of thrusts, thermal post-rift subsidence (Vacherat et al., 2014), basement heterogeneities in the retro-foreland basin (Angrand et al., 2018), geological and geometric complexities during mountain building (Vacherat et al., 2017), and lateral variations in exhumation and uplift of the mountain range (Curry et al., 2021; Fillon & van der Beek, 2012; Fitzgerald et al., 1999). However, several first order features of our models are useful to provide understanding of retro-foreland basins systems such as in the northern Pyrenees.

In our models, mean mountain range elevation after 25 Myr is in the order of 1.5–2 km (Figure 5a), similar to the reconstructed mean elevation of the Pyrenean mountain range at the end of the syn-orogenic phase (e.g., Curry et al., 2019; Huyghe et al., 2012). The maximum total subsidence at the deepest part of the Pyrenean retro-foreland (Central Pyrenees; close to ECORS line; Roure et al., 1989) ranges between 4 and 5 km-depth (Ford et al., 2016), which is to first order consistent with models presented here that include an initially deep foreland basin (models M3 and M4; Figures 6 and 9). The inherited bathymetry included here in models M3 and M4 represents pre-existing rift structure characteristic of many foreland basins worldwide including the Pyrenean retro-foreland (Desegaulx et al., 1991; Erdos et al., 2014; Vacherat et al., 2017).

A pre-existing deep foreland basin also explains some features of the retro-foreland basin of the northern Pyrenees, in particular the initially deep depositional environment in the foreland basin (flysch; Puigdefabregas & Souquet, 1986) with a significant marine sedimentary section (Serrano et al., 2006; Figure 10b). Models without an initially deep foreland reach basement depths shallower than the present-day basement in the Pyrenean retro-foreland (Figure 10c; Angrand et al., 2018). Reference model M1 produces a foreland basin thinner than in the North Pyrenean case and is filled only by shallow marine sediments during the underfilled phase (< 100 m-depth at time of deposition; Figure 6a). Model M2 does not preserve any marine sediments while the Pyrenean retro-foreland does (Figures 10b and 10c). In model M3, with an initially deep foreland basin, the basement is about 1 km deeper than in the Pyrenean case (Figure 10c), but, the stratigraphic architecture is consistent with the main trends of the present-day Pyrenean retro-foreland basin of Serrano et al. (2006) (Figure 10b and 10c). The initially deep basin in model M3, could be interpreted as a rift remnant, required to preserve a significant proportion of marine sediments in the foreland basin, and, more specifically deep marine sediments (> 300 m-depth at time of deposition; Figure 6c). These are consistent with the northern Pyrenean flysch, deposited during the late-Cretaceous, at the onset of the orogenic phase (Puigdefabregas & Souquet, 1986). We quantitatively show here that inherited bathymetry in foreland basins is critical to explain preservation of deep-marine sediments in small-scale orogen retro-foreland (Figures 9 and 10).

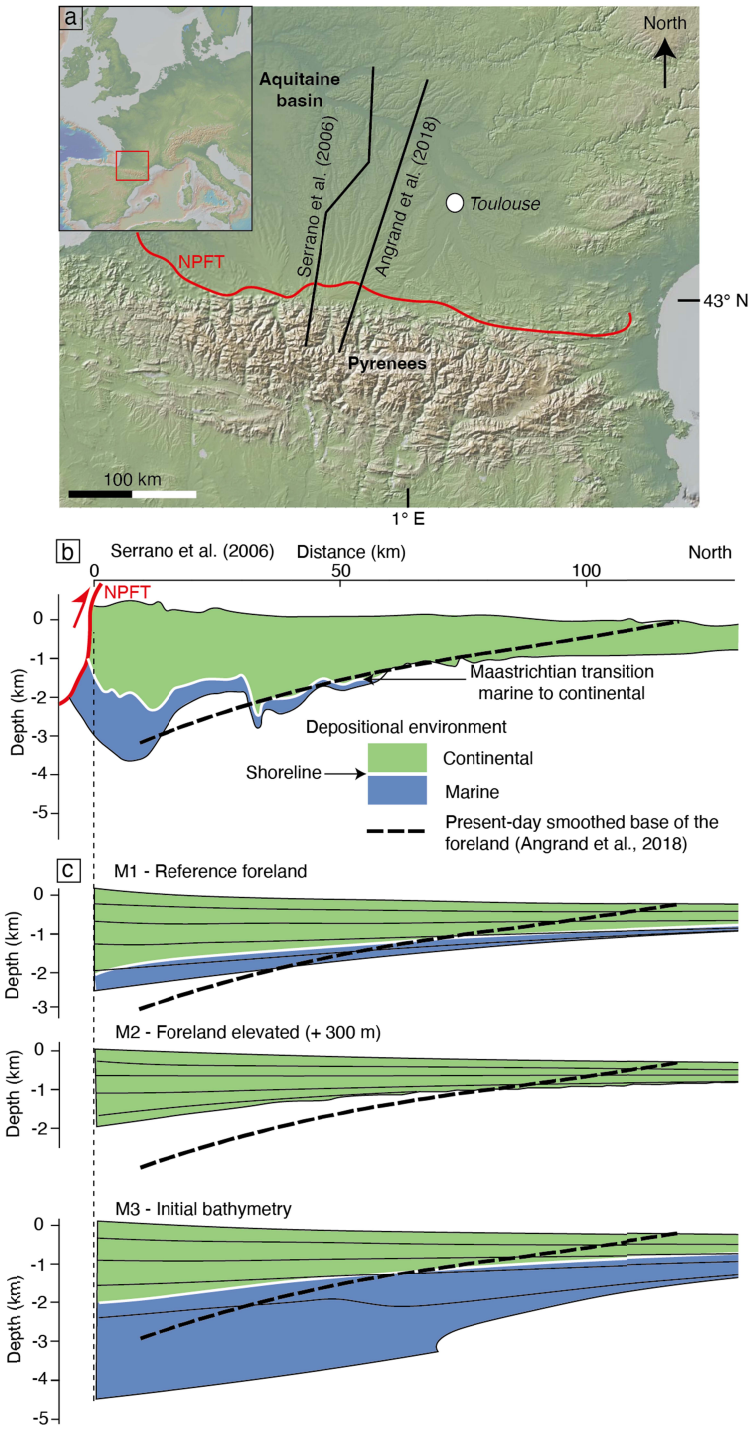

Figure 10. a) Pyrenees and cross-section locations (from Angrand et al. (2018) and Serrano et al. (2006). The inset shows Pyrenees and its associated Aquitaine foreland basin location (red square) at the scale of western Europe. b) Cross-section of the Pyrenean retro-foreland stratigraphy modified after Serrano et al. (2006). The transition from marine to continental depositional environment is deduced from Rougier et al. (2016). c) Cross-sections of foreland basin stratigraphic architectures and basement depth in models M1 to M3. We plotted the present-day smoothed base of the Pyrenean retro-foreland from Angrand et al. (2018). NPFT: Northern Pyrenean Frontal Thrust.

4.6 Model limitations

Thrust front propagation may affect the syn-orogenic dynamics of foreland basins (Simpson, 2006), in particular by remobilizing previously deposited sediments at the foot of the mountain range as well as inducing retrogradation phases in the foreland basin at the onset of thrusting events (Flemings & Jordan, 1990). These effects of thrust propagation are significant in pro-foreland systems where thrust front migration can exceed 100 km as for instance in the southern Pyrenean pro-wedge (Grool et al., 2018). Our models do not include horizontal deformation and cannot be used as an analogue for pro-wedge systems. However, they are useful for understanding retro-foreland systems of small to intermediate size orogens in which the maximum propagation of the deformation front is limited and less than 100 km. The northern Pyrenees are characterized by a shortening about 60 km (Grool et al., 2018). In retro-foreland basins, the stratigraphic architecture is mostly controlled by the load of mountain range topography and the associated flexural isostatic subsidence of the foreland the limited, whereas horizontal thrust propagation plays a subordinate role (Naylor & Sinclair, 2008).

Natural examples of mountain range-foreland systems may also display lateral variations in the degree of shortening, amount of erosion and corresponding sediment delivery to the foreland. In the case of the Pyrenees, the basement depth varies from 1-3 km in the east to > 5 km in the west. This variation has been mainly related to variations in extensional inheritance in the foreland (Angrand et al., 2018). The asymmetric and diachronous onset of the orogenic phase from east to west (Vacherat et al., 2017) is also responsible for along strike varying sediment supply range which impact the foreland basin filling and the stratigraphic architecture (Michael et al., 2014; Ortiz et al., 2022; Verges, 2007). Our cylindrical modelling setup does not allow to test for these lateral variations, that may be investigated in future work using a non-cylindrical model setup.

For sake of simplicity, in our models, global sea-level, precipitation rate, and continental transport coefficient (K_f) are constant through time and homogenous in space. Furthermore, we do not include a multi-grain size distribution of the marine deposition and marine diffusion of sediments (e.g., sand vs. silt; Rouby et al., 2013; Yuan et al., 2019b). Investigation of climate-driven variations of sediment flux is beyond the scope of our study. We focus on the long-term stratigraphic architecture of the foreland basin and the detailed stratigraphic architecture of the open-marine domain is beyond the scope of our study.

Finally, although our setup is cylindrical, the Fastscape S2S models result in three dimensional depositional systems at high-resolution and in lateral variations of deltas or alluvial fans at small-scale (Figure 4; Movies S1 to S4). However, these local sediment migrations along strike do not affect the long-term trends in the sedimentary filling and stratigraphic architecture.

5 Conclusions

We investigate the influence of inherited foreland relief on the stratigraphic evolution of the foreland domain during the building of a mountain range using a landscape evolution model that couples continental and marine surface processes with flexural isostasy. We show models with four characteristically different initial relief in the foreland domain: an initially foreland domain at sea-level, an initially +300 m high continental foreland, a pre-existing 1 km-deep and 100 km-wide foreland basin associated with either a forebulge at sea-level or elevated at +300 m.

The models show that after 25 Myr an initially elevated foreland domain produces a thinner foreland basin than a low-lying foreland domain because a larger proportion of sediments is exported out of the foreland domain to the open marine domain, which reduces the sedimentary load, the flexure and accommodation space creation in the foreland basin. In contrast, an initially deep foreland basin, produces a thicker foreland basin than an initial flat foreland domain because the sediments filling the initial space increase the load, the flexure and accommodation space in the foreland basin. In our model, an initially deep foreland basin is required to preserve a significant proportion of deep marine deposits in the foreland basin. Comparison with the Pyrenean retro-foreland basin shows that inherited bathymetry related to pre-orogenic rift structure, is required to preserve a significant amount of deep marine deposits often encountered in orogenic systems worldwide.

The results presented here illustrate how changes in the dynamics of the depositional system at the foot of the mountain range (fluvial deposits and alluvial fans) exert a feedback on the erosion of the mountain range. A transient drop of erosion rates occurs when continentalization and/or alluvial fan coalescence at the foot of the mountain range raise its local base level.

The models show that the influence of the inherited relief largely disappears after ~10-13 Myr and all models show similar landscapes with a continentalized foreland domain developing longitudinal hydrographic networks. However, even at 25 Myr the location of the shoreline provides a memory of the initial foreland basin setting. Flexural isostasy appears to become less important in the foreland stratigraphic evolution with time, when the forebulge is permanently buried by marine or continental sediments. However, the stratigraphic architecture of the foreland basin does provide information on the initial geometry, with the occurrence of deep marine sediments resulting from an initially deep foreland basin.

Acknowledgments

This work is part of the COLORS project, funded by Total. We thank Frederic Christophoul, Sebastian Wolf, Sébastien Carretier and Josep Anton Muñoz for constructive discussions while writing the manuscript.

Open Research

We use in this study a Landscape Evolution Model (FastScape S2S; Yuan et al., 2019a; Yuan et al., 2019b; https://fastscape.org); The version of the program we use is the one published online on April 26th 2021 (release v0.1.0beta3; fastscapelib-fortran; public access) available on GitHub: https://github.com/fastscape-lem.

References

Allen, P. A., & Allen, J. R. (2005). *Basin Analysis: Principles and Applications*. (Blackwell Science, Ed.) (Second edi).

Angrand, P., Ford, M., & Watts, A. B. (2018). Lateral Variations in Foreland Flexure of a Rifted Continental Margin: The Aquitaine Basin (SW France). *Tectonics*, *37*(2), 430–449. https://doi.org/10.1002/2017TC004670

Armitage, J. J., Dunkley Jones, T., Duller, R. A., Whittaker, A. C., & Allen, P. A. (2013).

Temporal buffering of climate-driven sediment flux cycles by transient catchment response. *Earth and Planetary Science Letters*, *369–370*, 200–210. https://doi.org/10.1016/j.epsl.2013.03.020

Babault, J., Bonnet, S., Crave, A., & Van Den Driessche, J. (2005). Influence of piedmont sedimentation on erosion dynamics of an uplifting landscape: An experimental approach. *Geology*, *33*(4), 301–304. https://doi.org/10.1130/G21095.1

Beaumont, C. (1981). Foreland basins. *Geophysical Journal of the Royal Astronomical Society*, (65), 291–329.

Bernard, T., Sinclair, H. D., Gailleton, B., Mudd, S. M., Ford, M., Recherches, C. De, et al. (2019). Lithological control on the post-orogenic topography and erosion history of the Pyrenees. *Earth and Planetary Science Letters*, *518*, 53–66. https://doi.org/10.1016/j.epsl.2019.04.034

Bovy, B. (2021). fastscape-lem/fastscape: Release v0.1.0beta3. https://doi.org/10.5281/ZENODO.4435110

Braun, J., & Willett, S. D. (2013). A very efficient O(n), implicit and parallel method to solve the stream power equation governing fluvial incision and landscape evolution. *Geomorphology*, *180–181*, 170–179. https://doi.org/10.1016/j.geomorph.2012.10.008

Bull, W. B. (1964). Geomorphology of segmented alluvial fans in western Fresno County, California. *U.S. Geological Survey, Professional Paper*, *352-E*, 89–129.

Carretier, S., & Lucazeau, F. (2005). How does alluvial sedimentation at range fronts modify the erosional dynamics of mountain catchments? *Basin Research*, *17*(3), 361–381. https://doi.org/10.1111/j.1365-2117.2005.00270.x

Catuneanu, O. (2004). Retroarc foreland systems – evolution through time. *Journal of African Earth Sciences*, *38*(7), 225–242. https://doi.org/10.1016/j.jafrearsci.2004.01.004

Catuneanu, O. (2019). First-order foreland cycles: Interplay of flexural tectonics, dynamic loading, and sedimentation. *Journal of Geodynamics*, *129*, 290–298. https://doi.org/10.1016/j.jog.2018.03.001

Clevis, Q., de Boer, P. L., & Nijman, W. (2004). Differentiating the effect of episodic tectonism and eustatic sea-level fluctuations in foreland basins filled by alluvial fans and axial deltaic systems: Insights from a three-dimensional stratigraphic forward model. *Sedimentology*, *51*(4), 809–835. https://doi.org/10.1111/j.1365-3091.2004.00652.x

Curry, M. E., van der Beek, P., Huismans, R. S., Wolf, S. G., & Muñoz, J. A. (2019). Evolving paleotopography and lithospheric flexure of the Pyrenean Orogen from 3D flexural modeling and basin analysis. *Earth and Planetary Science Letters*, *515*, 26–37. https://doi.org/10.1016/j.epsl.2019.03.009

Curry, M. E., van der Beek, P., Huismans, R. S., Wolf, S. G., Fillon, C., & Muñoz, J. A. (2021). Spatio-temporal patterns of Pyrenean exhumation revealed by inverse thermo-kinematic modeling of a large thermochronologic data set. *Geology*, *49*(6), 738–742. https://doi.org/10.1130/G48687.1

Davy, P., & Lague, D. (2009). Fluvial erosion/transport equation of landscape evolution models revisited. *Journal of Geophysical Research: Solid Earth*, *114*(3), 1–16. https://doi.org/10.1029/2008JF001146

DeCelles, P. G. (2012). Foreland basin systems revisited: variations in response to tectonic settings. In B. P. Ltd. (Ed.), *Tectonics of Sedimentary Basins: Recent Advances* (Blackwell, pp. 405–426).

DeCelles, P. G., & Giles, K. A. (1996). Foreland basin systems. *Basin Research*, *8*(2), 105–123.

https://doi.org/10.1046/j.1365-2117.1996.01491.x
Densmore, A. L., Allen, P. A., & Simpson, G. (2007). Development and response of a coupled catchment fan system under changing tectonic and climatic forcing. *Journal of Geophysical Research: Earth Surface*, *112*(1), 1–16. https://doi.org/10.1029/2006JF000474
Desegaulx, P., Kooi, H., & Cloetingh, S. (1991). Consequences of foreland basin development on thinned continental lithosphere: application to the Aquitaine basin (SW France). *Earth and Planetary Science Letters*, *106*, 116–132.
Dickinson, W. R. (1974, January 1). Plate Tectonics And Sedimentation. (W. R. Dickinson, Ed.), *Tectonics and Sedimentation*. SEPM Society for Sedimentary Geology. https://doi.org/10.2110/pec.74.22.0001
Erdos, Z., Huismans, R. S., van der Beek, P., & Thieulot, C. (2014). Extensional inheritance and surface processes as controlling factors of mountain belt structure. *Journal of Geophysical Research: Solid Earth*, *119*, 9042–9061. https://doi.org/10.1002/2014JB011408.Received
Fillon, C., & van der Beek, P. (2012). Post-orogenic evolution of the southern Pyrenees: Constraints from inverse thermo-kinematic modelling of low-temperature thermochronology data. *Basin Research*, *24*(4), 418–436. https://doi.org/10.1111/j.1365-2117.2011.00533.x
Fitzgerald, P. G., Muñoz, J. A., Coney, P. J., & Baldwin, S. L. (1999). Asymmetric exhumation across the Pyrenean orogen: Implications for the tectonic evolution of a collisional orogen. *Earth and Planetary Science Letters*, *173*(3), 157–170. https://doi.org/10.1016/S0012-821X(99)00225-3
Flemings, P. B., & Jordan, T. E. (1989). A Synthetic Stratigraphic Model of Foreland Basin Development. *Journal of Geophysical Research*, *94*(B4), 3851–3866.
Flemings, P. B., & Jordan, T. E. (1990). Stratigraphic modeling of foreland basins: Interpreting thrust deformation and lithosphere rheology. *Geology*, *18*(5), 430–434. https://doi.org/10.1130/0091-7613(1990)018<0430:SMOFBI>2.3.CO;2
Ford, M. K., Hemmer, L., Vacherat, A., Gallagher, K., & Christophoul, F. (2016). Retro-wedge foreland basin evolution along the ECORS line, eastern Pyrenees, France. *Journal of the Geological Society*, *173*(3), 419–437. https://doi.org/https://doi.org/10.1144/jgs2015-129
Garcia-Castellanos, D., & Cloetingh, S. (2012). Modeling the Interaction between Lithospheric and Surface Processes in Foreland Basins. In C. Busby & A. Azor (Eds.), *Tectonics of Sedimentary Basins: Recent Advances* (First Edit, pp. 152–181). Blackwell Publishing Ltd. https://doi.org/10.1002/9781444347166.ch8
Grool, A. R., Ford, M., Vergés, J., Huismans, R. S., Christophoul, F., & Dielforder, A. (2018). Insights Into the Crustal-Scale Dynamics of a Doubly Vergent Orogen From a Quantitative Analysis of Its Forelands: A Case Study of the Eastern Pyrenees. *Tectonics*, *37*(2), 450–476. https://doi.org/10.1002/2017TC004731
Grool, A. R., Huismans, R. S., & Ford, M. (2019). Salt décollement and rift inheritance controls on crustal deformation in orogens. *Terra Nova*, *31*(6), 562–568. https://doi.org/10.1111/ter.12428
Guerit, L., Yuan, X. P., Carretier, S., Bonnet, S., Rohais, S., Braun, J., & Rouby, D. (2019). Fluvial landscape evolution controlled by the sediment deposition coefficient: Estimation from experimental and natural landscapes. *Geology*, *47*(9), 853–856. https://doi.org/10.1130/G46356.1
Heller, P. L., Angevine, C. L., Winslow, N. S., & Paola, C. (1988). Two-phase stratigraphie model of foreland-basin sequences. *Geology*, *16*(June), 501–504.

766 Huyghe, D., Mouthereau, F., & Emmanuel, L. (2012). Oxygen isotopes of marine mollusc shells
767 record Eocene elevation change in the Pyrenees. *Earth and Planetary Science Letters*, *345–*
768 *348*, 131–141. https://doi.org/10.1016/j.epsl.2012.06.035
769 Jordan, T. E., & Flemings, P. B. (1991). Large-Scale Stratigraphic Architecture, Eustatic
770 Variation, and Unsteady Tectonism: A Theoritical Evaluation. *Journal of Geophysical*
771 *Research*, *96*(B4), 6681–6699.
772 Michael, N. A., Whittaker, A. C., Carter, A., & Allen, P. A. (2014). Volumetric budget and
773 grain-size fractionation of a geological sediment routing system: Eocene Escanilla
774 Formation, south-central Pyrenees. *Bulletin of the Geological Society of America*, *126*(3–4),
775 585–599. https://doi.org/10.1130/B30954.1
776 Milana, J. P., & Ruzycki, L. (1999). Alluvial-fan slope as a function of sediment transport
777 efficiency. *Journal of Sedimentary Research*, *69*(3), 553–562.
778 https://doi.org/10.2110/jsr.69.553
779 Molnar, N., & Buiter, S. (2022). Analogue modelling of inversion tectonics: investigating the
780 role of multiple extensional basins in foreland fold-and-thrust belts. In *EGU General*
781 *Assembly 2022* (pp. EGU22-7027). Vienna, Austria. Retrieved from
782 https://doi.org/10.5194/egusphere-egu22-7027
783 Naylor, M., & Sinclair, H. D. (2008). Pro- vs . retro-foreland basins. *Basin Research*, *20*, 285–
784 303. https://doi.org/10.1111/j.1365-2117.2008.00366.x
785 Ortiz, A., Guillocheau, F., Lasseur, E., Briais, J., Robin, C., Serrano, O., & Fillon, C. (2020).
786 Sediment routing system and sink preservation during the post-orogenic evolution of a
787 retro-foreland basin: The case example of the North Pyrenean (Aquitaine, Bay of Biscay)
788 Basins. *Marine and Petroleum Geology*, *112*(October 2019), 104085.
789 https://doi.org/10.1016/j.marpetgeo.2019.104085
790 Ortiz, A., Guillocheau, F., Robin, C., Lasseur, E., Briais, J., & Fillon, C. (2022). Siliciclastic
791 sediment volumes and rates of the North Pyrenean retro-foreland basin. *Basin Research*,
792 (March), 1–19. https://doi.org/10.1111/bre.12665
793 Paola, C. (2000). Quantitative models of sedimentary basin filling. *Sedimentology*, *47*, 121–178.
794 Puigdefabregas, C., & Souquet, P. (1986). Tecto-sedimentary cycles and depositional sequences
795 of the Mesozoic and Tertiary from the Pyrenees. *Tectonophysics*, *129*, 173–203.
796 Rouby, D., Braun, J., Robin, C., Dauteuil, O., & Deschamps, F. (2013). Long-term stratigraphic
797 evolution of Atlantic-type passive margins: A numerical approach of interactions between
798 surface processes, flexural isostasy and 3D thermal subsidence. *Tectonophysics*, *604*, 83–
799 103. https://doi.org/10.1016/j.tecto.2013.02.003
800 Rougier, G., Ford, M., Christophoul, F., & Bader, A. G. (2016). Stratigraphic and tectonic
801 studies in the central Aquitaine Basin, northern Pyrenees: Constraints on the subsidence and
802 deformation history of a retro-foreland basin. *Comptes Rendus - Geoscience*, *348*(3–4),
803 224–235. https://doi.org/10.1016/j.crte.2015.12.005
804 Roure, F., Choukroune, P., Berastegui, X., Munoz, J. A., Villien, A., Matheron, P., et al. (1989).
805 ECORS deep seismic data and balanced cross sections: Geometric constraints on the
806 evolution of the Pyrenees. *Tectonics*, *8*(1), 41–50.
807 Schlunegger, F., Jordan, T. E., & Klaper, E. (1997). Controls of erosional denudation in the
808 orogen on foreland basin evolution : The Oligocene central Swiss Molasse Basin as an
809 example. *Tectonics*, *16*(5), 823–840.
810 Serrano, O., Delmas, J., Hanot, F., Vially, R., Herbin, J.-P., Houel, P., & Tourlière, B. (2006). Le
811 Bassin d'Aquitaine: valorisation des données sismiques, cartographie structurale et potentiel

pétrolier. *Edition BRGM*, 245.
Simon, B., Robin, C., Rouby, D., Braun, J., & Guillocheau, F. (n.d.). *Rifted margin stratigraphy provides calibration of marine diffusion coefficient: measurements in the Ogooué and Zambezi deltas (in revision for Basin Research)*.
Simpson, G. (2014). Decoupling of foreland basin subsidence from topography linked to faulting and erosion. *Geology*, *42*(9), 775–778. https://doi.org/10.1130/G35749.1
Simpson, G. D. H. (2006). Modelling interactions between fold-thrust belt deformation, foreland flexure and surface mass transport. *Basin Research*, *18*(2), 125–143. https://doi.org/10.1111/j.1365-2117.2006.00287.x
Sinclair, H. D., Coakley, B. J., Allen, P. A., & Watts, A. B. (1991). Simulation of foreland basin stratigraphy using a diffusion model of mountain belt uplift and erosion: An example from Central Alps, Switzerland. *Tectonics*, *10*(3), 599–620.
Stock, J. D., & Montgomery, D. R. (1999). Geologic constraints on bedrock river incision using the stream power law. *Journal of Geophysical Research: Solid Earth*, *104*(B3), 4983–4993. https://doi.org/10.1029/98jb02139
Theunissen, T., Huismans, R. S., Lu, G., & Riel, N. (n.d.). *Relative continent/mid-ocean ridge elevation: a reference case for isostasy in geodynamics (in revision for Earth-Science Reviews)*.
Vacherat, A., Mouthereau, F., Pik, R., Bernet, M., Gautheron, C., Masini, E., et al. (2014). Thermal imprint of rift-related processes in orogens as recorded in the Pyrenees. *Earth and Planetary Science Letters*, *408*, 296–306. https://doi.org/10.1016/j.epsl.2014.10.014
Vacherat, Arnaud, Mouthereau, F., Pik, R., Huyghe, D., Paquette, J. L., Christophoul, F., et al. (2017). Rift-to-collision sediment routing in the Pyrenees: A synthesis from sedimentological, geochronological and kinematic constraints. *Earth-Science Reviews*, *172*(July), 43–74. https://doi.org/10.1016/j.earscirev.2017.07.004
Verges, J. (2007). Drainage responses to oblique and lateral thrust ramps: a review. In G. Nichols, C. Paola, & E. Williams (Eds.), *Sedimentary Processes, Environments and Basins: A Tribute to Peter Friend* (IAS Spec., pp. 29–47). Blackwell Publishing. https://doi.org/10.1002/9781444304411.ch3
Whipple, K. X., & Tucker, G. E. (1999). Dynamics of the stream-power river incision model: Implications for height limits of mountain ranges, landscape response timescales, and research needs. *Journal of Geophysical Research*, *104*, 661–674.
Willett, S., Beaumont, C., & Fullsack, P. (1993). Mechanical model for the tectonics of doubly vergent compressional orogens. *Geology*, *21*(4), 371–374. https://doi.org/10.1130/0091-7613(1993)021<0371:MMFTTO>2.3.CO;2
Wolf, S. G., Huismans, R. S., Muñoz, J. A., Curry, M. E., & van der Beek, P. (2021). Growth of Collisional Orogens From Small and Cold to Large and Hot—Inferences From Geodynamic Models. *Journal of Geophysical Research: Solid Earth*, *126*(2), 1–32. https://doi.org/10.1029/2020JB021168
Yuan, X. P., Braun, J., Guerit, L., Rouby, D., & Cordonnier, G. (2019a). A New Efficient Method to Solve the Stream Power Law Model Taking Into Account Sediment Deposition. *Journal of Geophysical Research: Earth Surface*, *124*(6), 1346–1365. https://doi.org/10.1029/2018JF004867
Yuan, X. P., Braun, J., Guerit, L., Simon, B., Bovy, B., Rouby, D., et al. (2019b). Linking continental erosion to marine sediment transport and deposition: A new implicit and O(N) method for inverse analysis. *Earth and Planetary Science Letters*, *524*, 1–15.

858 https://doi.org/10.1016/j.epsl.2019.115728
859